A Novel DE algorithm for solving dynamic OPF for expected security cost incorporating solar and flexible resources in smart grids

B. Aruna Kumari[1*], K. Vaisakh[2], N.C.Sahoo[3]

[1*] Department of Electrical Engineering, Andhra University College of Engineering (A), Visakhapatnam-530003, A.P, India.
[2] Department of Electrical Engineering, Andhra University College of Engineering (A), Visakhapatnam-530003, A.P, India.
[3] School of Electrical Sciences, Indian Institute of Technology, Bhubaneswar-752050, ODISHA, India.

* Corresponding author

Abstract--Significant amount of solar electricity generation enhances the attributes in terms global environmental, national energy security concerns and rising fuel prices. Thus, the integration of solar based power generations, combined with the dwindling fossil fuel generation and rapidly changing energy demand, creates major operational and security challenges for modern power systems. This paper proposes an Expected-Security-Cost-with Dynamic Optimal Power Flow (ESC-DOPF) model by incorporating solar resources and flexible resources (FRs) with a Modified Differential Evolution (MDE) optimization algorithm to obtain the global solution for the total expected operation cost under normal and post-contingency states by satisfying the model constraints over a given 24-hour time horizon. Beta probability distribution function is considered for optimal scheduling of solar power generation. Similarly, FRs such as demand response, battery energy storage systems, and HVDC systems are also modelled to maintain the supply-demand portfolio at every moment. Various scenarios are tested on a modified IEEE-30 bus system to validate the proposed algorithm. Results show that the proposed MDE algorithm satisfies all of the operational constraints and also provides cost savings from the integration of solar and FRs into the power system.

Keywords: Dynamic optimal power flow, expected security cost, flexible resources, HVDC transmission, new DE algorithm, solar resources and modelling.

1 Introduction

With the increased use of variable renewable energy (VRE) helps countries meet their targets of energy security and emission reduction [1]. Global power systems have concentrated on three main roles: generating, transmitting, and distributing energy as a real-time commodity. Physics implies that, considering fluctuations in load on timescales ranging from sub-second fluctuations to multi-year patterns, electricity generation is still in real-time balance with load. Conversely, with the growing role of variable solar generation, the dwindling fossil fuel generation, and the shifting profile of consumer demand, will create several challenges for energy systems.

The objective of modern power system operations is to securely dispatch and efficiently serve the load while integrating diverse generation technologies. Optimal power flow (OPF) is an important issue in power system dispatching and security. The OPF model faces the challenge of balancing the needs of the transmission network while minimizing operating costs [2]–[3]. In [4], the authors proposed dynamic optimal power flow (DOPF), an extended method for solving OPF over a time horizon by incorporating inter-temporal constraints. The AC security-constrained OPF (SCOPF) [5]–[6] is a tool for ensuring N-1 security that is primarily used in day-to-day operations to procure ancillary services. Based on the SCOPF paradigm, there are two methods, i.e., preventive SCOPF and corrective SCOPF. Several literature reviews have been carried out to enhance security against the state of post-contingency in both preventive and corrective SCOPFs [7]–[8]. A systematic formulation that minimizes the total expected operating cost, the post contingency generation rescheduling and load interruption costs, minus the customer benefits. To solve the model with dc approximation, the primal-dual interior-point (PDIP) algorithm is used [9]. This model was later extended to include AC networks and flexible alternating current transmission system (FACTS) allocation with small-signal stability constraints [10]–[11]. Because of environmental concerns and recent energy shortages, the incorporation of renewable energy resources (RERs) is becoming more popular [12]. The management of uncertainty and variability in the RER is a crucial challenge due to the stochastic nature. Thus, extant literature reveals that several literature studies have been reported on the formation of economic load dispatch (ELD) [13]–[15], OPF and SCOPF with RER using different heuristic algorithms. In [16], dynamic ELD problem with RERs using improved fireworks algorithm. The detailed OPF formulation with RER including wind and solar is provided in [17]–[21]. To describe the inherent variability in wind speed and solar irradiance behavior, most research utilized the probability distribution function (PDF) [22], which incorporated the uncertainty costs associated with RER power generation in the OPF [23]–[24]. A multi-objective hybrid algorithm to solve security constrained optimal power flow (SCOPF) with wind and conventional generators under contingencies is presented in [25]. A multi-period stochastic SCOPF considering different uncertainty sources is available in [26]. In [27], a fuzzy based optimization algorithm that considers wind and thermal generators to solve SCOPF is presented.

The electricity market creates a flexible resource (FR) for operating a secure and reliable system in real-time situations due to the continuous increase in demand and rapid development of the smart grid [28]. Demand response (DR)/demand side management (DSM), battery-energy storage-systems (BESS) and high-voltage direct-current (HVDC) systems are commonly used FR to enhance security and reliability. Based on earlier studies, developing energy management systems for power networks that integrate smart energy resources is becoming increasingly popular [29]–[30]. DR manages demand by offering economic benefits based on supply and demand. The smart grid uses DR to save energy by visualizing power consumption and managing load by changing electricity tariffs based on time zone [31]–[32]. The authors in [33] suggested that DR programs contribute to reliability measures during emergencies. In [34]–[35], the authors proposed a power grid's dynamic economic and emission dispatch (DEED) and DOPF with DR. This DEED and DOPF model with DR combination was primarily designed to benefit both the utility and generation sides. In [36], A DR program integrated with ELD problem including RER using a heuristic algorithm. BESS is a form of scalable resource that has recently piqued the interest of researchers, system operators, and end-users [37]–[39].

Due to the rapid decline in the cost of storage technologies, especially lithium-ion batteries, the role of battery storage in a power system has gained prominence [40]. Its main purpose is to conserve the stored resources and it plays a key role in ensuring that supply-demand portfolio is balanced at all times. The BESS is mainly concerned with energy efficiency in order to reduce costs and increase revenue while maintaining flexibility. As part of the solution to the SCOPF, the authors of [41]–[42] propose that batteries operate in the post-contingency corrective control state. In [43], the authors studied the DOPF problem of active distribution networks containing RER, flexible demand and energy storage systems (ESS) in an active network management context. In [44], a stochastic MP-SCOPF with flexible loads and ESS to provide flexibility for regulating congestion and voltages has been proposed.

Due to the grid's controllability and reliability by enabling transmission over longer distances with less power loss, the line commutated converters (LCC)-HVDC systems seem to be the most secure and cost effective choice [45]–[48]. In [49]–[50], the authors propose multi-period OPF with HVDC connected wind farms. In [51], describe a decoupled way of computing multi-period (MP) SCOPF that covers both N-1 security criteria and quasi-stationary dynamics in smart grids with ESS via interconnected area coordination.

Few authors attempting to extend AC SCOPF have analyzed emerging sources of flexibility in conjunction with solar uncertainties. Despite these encouraging developments, this paper proposes a new mathematical approach for extending the MP-SCOPF model by treating security as an economic cost rather than a constraint, colloquially referred to as "expected security cost DOPF" (ESC-DOPF), to minimize expected system operating costs under pre-and post-contingencies. To the best of the authors' knowledge, the researchers have not addressed the formulation of the problem in the form of an MP-ESCOPF or ESC-DOPF with the integration of solar resources and FR. The stochastic nature of solar is modeled through Beta PDF [16]–[17]. The proposed model is examined to demonstrate how the DR manages generation and load based on residential users' controllable loads. A game-theory based energy consumption and day-ahead pricing (DAP) strategy are implemented [34–35]. To improve the system reliability, BESS is also applied to the proposed model. Furthermore, the authors developed a unified Newton-Raphson (NR) based two-terminal line commutated converter (LCC)-HVDC system [45–50] that can be applied to the ESC-DOPF model. Evolutionary algorithms are capable of effectively solving the proposed model.

Evolutionary algorithms are capable of effectively solving the proposed model. In recent decades, Storn and Price (1995) differential evolution (DE) algorithm has established itself as a powerful population-based stochastic search algorithm for finding a globalised solution with good global search capability and few or no cost function constraints [52–54]. Thus, several empirical studies [55–58] have backed up the findings of solving small-scale optimization problems. However, when dealing with optimization problems that are complex multimodal and have a high dimensionality (>200), the DEs variants fail miserably. This is because, due to some inherent internal difficulties, striking a balance between algorithm convergence (local extraction power) and population diversity (global exploring power) is extremely difficult. To overcome this issue, presented in this work is a new crossover operator as well as a new local control strategy. To maintain a strong global search capacity, a high value of crossover probability and an adjustment step are used in the early search process. Later in the evolution cycle, a low crossover rate combined with a fine-tuning technique is used to increase local exploitation capacity [59]. Therefore, a "modified differential evolution" (MDE) algorithm is proposed to work out the ESCDOPF problem with solar and FR during pre-and post-contingencies. Also, the economic benefits of incorporating solar and FR into the ESCDOPF model are assessed.

The rest of the paper is arranged as: Section 2 presents the formulations of the ESCDOPF model with solar and FR. Section 3 focuses on the solution methodology. Section 4provides test system data. Section 5 represents the simulation results with discussions, respectively. Finally, Section 6 contains the conclusions.

2 Formulation of ESCDOPF with solar and FR

The detailed mathematical modelling of the proposed ESCDOPF with solar and FR is discussed in this section.

2.1 Modelling of solar resources

There are several models for solar irradiance, but the Beta probability density function (PDF) is most preferred model which utilizes the solar radiation. The output of a PV generator can be found in [16].

The probability of solar irradiance (G_s) can be calculated by Beta PDF ($f_{G_s}(G_s)$) as follows [16]:

$$f_{G_s}(G_s)=\begin{cases}\dfrac{\Gamma(a_s+b_s)}{\Gamma(a_s)\Gamma(b_s)}\left(\dfrac{G_s}{G_{max,s}}\right)^{a_s-1}\left(1-\dfrac{G_s}{G_{max,s}}\right)^{b_s-1} ; \ for\ \ 0\le\left(\dfrac{G_s}{G_{max,s}}\right)\le 1, \quad a_s>0, b_s>0, \\ 0\ ;\ \ Otherwise\end{cases} \tag{1}$$

where the a_s and b_s are the beta parameters with mean μ_s and standard deviation σ_s is as follows

$$a_s=\mu_s^2\left(\frac{1-\mu_s}{\sigma_s^2}-\frac{1}{\mu_s}\right); \ b_s=a_s\left(\frac{1}{\mu_s}-1\right) \tag{2}$$

Since, Beta distribution variable lie in the range of (0, 1). Hence, a nominal value of solar irradiance is (G_s/ $G_{max,s}$) considered. where $G_{max,\,s}$ is the maximum solar irradiance. Further, the solar irradiance to energy conversion for solar is given by:

$$f_{G_s}(P_s)=\begin{cases}\dfrac{1}{P_{max,s}}\dfrac{\Gamma(a_s+b_s)}{\Gamma(a_s)\Gamma(b_s)}\left(\dfrac{P_s}{P_{max,s}}\right)^{a_s-1}\left(1-\dfrac{P_s}{P_{max,s}}\right)^{b_s-1} ; \text{for}\ \ 0\le\left(\dfrac{P_s}{P_{max,s}}\right)\le 1, \quad a_s>0, b_s>0, \\ 0;\ \ otherwise\end{cases} \tag{3}$$

where $P_{max,s}$ is the maximum generated solar power; P_s is the solar power.

2.2 Game theory-basedDemand Response model

Demand response (DR) is one of the flexible resources used during peak load hours to determine the desired load profile based on lower energy consumption and consumer price levels. This could lead to changes in the shape of the actual forecasted utility load. Peak-clipping, load-shifting, strategic load growth, flexible load shape, strategic conservation, and valley-filling are six possible general load shapes that may be used to conduct demand-side operations, as depicted in **Fig. 1.** In this paper, a day-ahead load-shifting DR strategy is implemented based on the Nash equilibrium energy consumption game theory algorithm among residential customers with different participation levels (PLs) [35]. The forecast load demand curve is taken from [4] for this purpose.

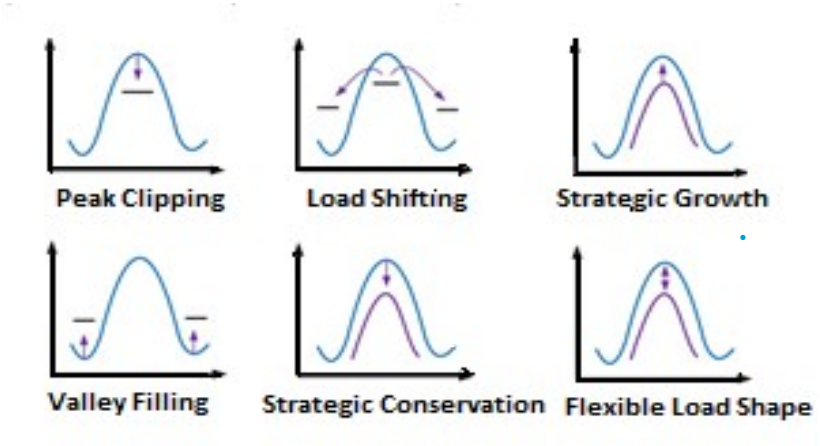

Fig. 1DRload shape measures

For example, consider a scheme with a single utility company and a large number of residential customers or users as depicted in **Fig. 2**.Each customer has a smart energy metre with an embedded energy-consumption-scheduler (ECS) that controls how the appliances in their home are scheduled. The ECS communicates with the utility provider via a two-way communication network that allows price information and the user's load demand to be exchanged.The utility company forecasts the demand for electricity one day ahead of time and sets the rates for each hour before enabling the schedule. The service provider then communicates these rates to all customers through a communication protocol. Then, based on the price information obtained from the utility provider, each customer optimises their energy usage by following the best scheduling for their appliances. Thus, the overall system energy bill is reduced while also improving system performance. In this energy consumption game, the nash equilibrium game approach is used. As a result, user deception and cheating can be avoided during their interaction.

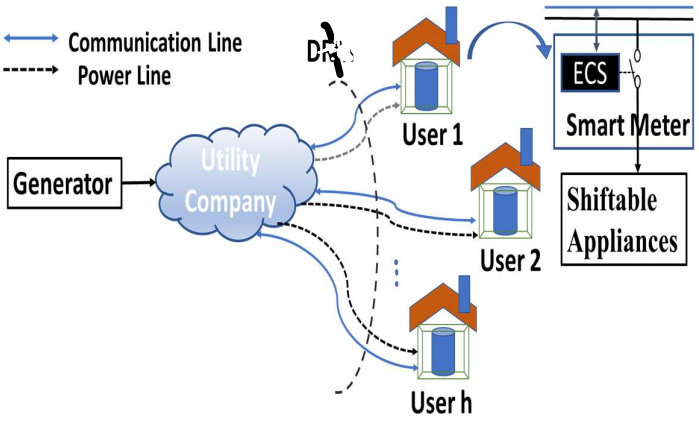

Fig. 2 Game theory-based DR Scenario.

The mathematical modelling is as follows:

Let us designate the group of N households by $N = \{1, \ldots, N\}$. For each household $n \in N$, let D_n^t denote the total demand at the time $t \in T = \{1, \ldots, T\}$ of T equivalent time slots, where T=24. Let a household's collection of appliances be denoted as $A_n = \{1, \ldots, A_n\}$. As a scheduling vector, the energy consumption of each appliance $a \in A_n$ is '$v_{n,a}$' and aoverall load demand of user $n \in N$ is provided as

$$P_{L,t} = \sum_{n \in N} D_n^t \tag{4}$$

where $D_n^t = \sum_{a \in A_n} v_{n,a}^t$

The predetermined average daily energy consumption for each household $n \in N$ and appliance $a \in A_n$ is represented as $E_{n,a}$. It is worth emphasising that the scheduler does not modify the quantity of energy utilized; instead, it uses the load shifting process to manage loads in a systematic manner. In this case, the user must decide the start $a_{n,a} \in T$ and end $b_{n,a} \in T$ of a time frame over which the appliance can be scheduled. For all appliances, the scheduling vector is thus bound to a constraint as $v_{n,a}^t$. Furthermore, we state that

$$\sum_{t=\alpha_{n,a}}^{\beta_{n,a}} v_{n,a}^t = E_{n,a} \tag{5}$$

$$v_{n,a}^t = 0, \quad \forall t \in T \setminus T_{n,a}; T_{n,a} = \{\alpha_{n,a}, \ldots\ldots, \beta_{n,a}\}$$

The basic purpose of the energyconsumption game is to minimise all the user's energy costs, which can be stated as

$$\min_{v_n, \forall n \in N} \text{minimize} \sum_{t \in T} C_t \tag{6}$$

Thus, through the conception of required new demand ($P_{L,t}$), which will be an outcome of ourapproach, the time of usage (TOU) rate tariff should be designed carefully to encourage users to follow the same profile. The flat-rate tariff model [29] isused to calculate the utility's energy cost, which is expressed as

$$C_t = a_t^p * P_{L,t} \tag{7}$$

where a_t^p is the tariff-constant.

For each household $n \in N$, let d_n denote the daily dollar billing amount to be charged by the utility to users at the end of each day. The amount received from users for electricity billing should normally be greater than or equal to the amount charged to the generating company for utility energy billing. In mathematical terms,

$$\sum_{n \in N} d_n = \sum_{t \in T} C_t \tag{8}$$

and

$$s @ \frac{\sum_{n \in N} d_n}{\sum_{t \in T} C_t} \geq 1 \tag{9}$$

If $s = 1$, the billing scheme is budget-balanced, and the utility company can make no profit. If $s > 1$, the power company would earn a benefit from the difference between the amount charged to the generator and the total amount received from the users. For analytical simplicity, the budget balanced billing scheme is employed in this paper. For solving each user's local optimization problem, a linear-integer programming (LIP) toolbox available in MATLAB is utilized and also summarised in **Algorithm 1** in a distributed fashion [35].

Algorithm1: *DRalgorithm executed by each household* $n \in N$ *in a distributed fashion*

---

1. Randomly initialize the load scheduling of n^{th} users as $\mathbf{v}_n$ *and all other remaining users other than n^{th} users as* $\mathbf{v}_{-n}$ *randomly.*
2. Repeat again
3. In instances of random time, ***do***
4. Solve an Eq. (6) using a linear-integer program
5. ***if*** *the value of* $\mathbf{v}_n$ *differs from the current schedule,* ***then***
6. Update $\mathbf{v}_n$ *and notify other users of the information*
7. ***endif***
8. ***if*** *any announcement/message is received,* ***then***
9. Update the corresponding $\mathbf{v}_{-n}$ *value*
10. ***endif***
11. Repeat the process up to no ECS announcements

2.3 Battery energy storage systems (BESS)

For the sake of simplicity, BESS is lossless and operates at a unity power factor. In this model, three modes of operation have been considered [37–38]. In the first mode, excess generation charges the battery, which acts as a load. Assuming there is no battery, generation equals demand, and the battery remains saturated at its maximum/minimum state-of-charge (SOC) levels. To meet demand in the third mode, the battery discharges and acts as a generator. The SOC is determined by multiple time steps of charge and discharge values.

The following are the battery charging and discharging equations [38] as:

$$SOC_{b,t}^{k} = \begin{cases} SOC_{b,t}^{ini,k}, & t = 1 \\ SOC_{b,t-1}^{k} + \left(U_{ch_b,t-1} * P_{ch_b,t-1}^{k} * \eta_{ch_b} \right) - \left(U_{dch_b,t-1} * \frac{P_{dch_b,t-1}^{k}}{\eta_{dch_b}} \right) \Delta t, & b \in N_{batt}, t > 1 \end{cases} \tag{10}$$

$$\sum_{t} P_{dch_b,t}^{k} \Big/ \eta_{dch_b} - \sum_{t} P_{ch_b,t}^{k} \cdot \eta_{ch_b} = 0 \quad \forall k \in (0,1,....,K) \tag{11}$$

$$U_{ch_b,t} + U_{dch_b,t} \leq 1, \ \forall \ b, \ t \tag{12}$$

The energy stored inside the battery at each time interval t is given in (10). Whereas Eq. (11) is used to distinct each day from the others. Eq. (12) defines the ability to load or unload at the same time.Here, k=0 and k>0 indicate the pre/normal contingency(C) state and post-contingency (C) states; K is the total number of contingencies; $P_{ch_b,t}^{k}$ and $P_{dch_b,t}^{k}$ are the b^{th} battery-charging (ch) and discharging (dch) powers of the k^{th} contingency state at time t respectively. $U_{ch_b,t}$ / $U_{dch_b,t}$ are the battery charging /discharging status. η_{ch_b} and η_{dch_b} are the charging and discharging efficiencies.

2.4 Unified LCC based HVDC system

In this study, a unified HVDC approach based on the Newton-Raphson (NR) algorithm with two-terminal (TT) line commutated converter (LCC) configurations is developed for evaluating power flow in an ESCDOPF model. In this model, the AC and DC power flow solutions can be solved simultaneously by the NR algorithm with a modified jacobian matrix [48]. The power flow equations of AC-DC systems are briefly describedin the following subsection for rapid reference. The complete unified power flow model can be simplified using first order Taylor expansion is given as:

$$\Delta F_{ac-dc}^{k} = -J_{ac-dc}^{k}\ \Delta X_{ac-dc}^{k} \tag{13}$$

Where ΔF_{ac-dc}^{k} is the residual of AC to DC system power flow equations; J_{ac-dc}^{k} are the jacobian matrix of ΔF_{ac-dc}^{k}; ΔX_{ac-dc}^{k} are the corrections for the AC to DC solutions, respectively.

2.5 Objective function

The classic ESCOPF formulation, which was originally proposed in [9], is adopted in this paper. This classicapproach, however, implies that control operations do not change during an emergency. Many resources, such as wind and FR, have recently been implemented in the system since their inclusion can operate as a preventive control measure during contingency periods and improve the system's performance in a safe, reliable, and economical manner. The main objective is to minimise the expected system operating cost by satisfying the model constraints in transmission network operation under both normal and post-contingency states.

This ESCDOPF problem can be abstractly and generically formulated as follows:

$$\min_{C^{k}}\left\{ESC=\left(\sum_{k=0}^{K}\sum_{t=1}^{T}\pi^{k}\ \mathrm{C}^{k}\left(t\right)\right)\right\}\ \ \forall k=\left\{0,1,.....K\right\} \tag{14}$$

where $C^{k}\left(t\right)$ is the expected operating cost, which includes pre/normal and post-contingency operating costs over a time interval T; The term "expected" is used in a probabilistic manner, and it applies to all contingencies; The probability of a contingency k is denoted as π^{k} [10].

The ESCDOPF problem with different cost models can be explicitly expressed as follows:

$$\mathrm{C}^{\mathrm{k}}\left(\mathrm{t}\right)=\underbrace{\mathrm{C}_{\mathrm{G_i}}(\mathrm{P}_{\mathrm{G_i,t}}^{\mathrm{k}})}_{\mathrm{GC}}+\underbrace{\mathrm{C}_{\mathrm{s}}(\mathrm{P}_{\mathrm{s,t}}^{\mathrm{k}})}_{\mathrm{SC}}+\underbrace{\mathrm{H}_{\mathrm{b}}(\mathrm{SOC}_{\mathrm{b,t}}^{\mathrm{k}})}_{\mathrm{BC}}\ -\underbrace{\mathrm{B}_{\mathrm{L_i}}(\mathrm{P}_{\mathrm{L_i,t}}^{\mathrm{k}})}_{\mathrm{CC}} \tag{15}$$

2.6 Cost Models:

2.6.1 Generator cost (GC) model

In this model, the valve point effects are considered. The valve loading effect is modelled as an absolute value with a sinusoidal function, which is then applied to the quadratic cost function [4] as,

$$GC=C_{G_i}(P_{G_i,t}^{k})=\sum_{t=1}^{T}\sum_{i=1}^{N_G}\left(a_{G_i}\left(P_{G_i,t}^{k}\right)^{2}+b_{G_i}P_{G_i,t}^{k}+c_{G_i}+\left|d_{G_i}\cdot sin(e_{G_i}(P_{G_i}^{\min}-P_{G_i}^{k}))\right|\right) \tag{16}$$

Where a_{G_i}, b_{G_i}, c_{G_i}, d_{G_i} and e_{Gi} are the coefficients of generator (G) cost functions with valve loading effect. $P_{G_i,t}^{k}$ is the output power of the ith generating unit of kth contingency at time 't' in MW. $P_{G_i}^{\min}$ is the generating unit's minimum real power in MW; $\mathrm{N_G}$ is the number of generating units.

2.6.2 Solarcost (SC) model

In this model,to incorporate the uncertain effect, the operating costs of solar generators include direct solar cost, underestimation/penalty cost and overestimation/ reserve cost. Solar power has a direct cost associated to it. When the cost of underestimation is taken in to account, the available solar power is more than the estimated solar power. But at an overestimation cost, the available solar power is less than the estimated solar power. Therefore, penalties have been introduced for the unused power. The solar operating cost ($C_s(P_{s,t}^{k})$) of sthsolar generator to generate solar power ($P_{s,t}^{k}$ MW) at time interval 't' with '$\mathrm{N_S}$' number of solar-generating units can be described [16] as,

$$SC = C_s(P_{s,t}^k) = \sum_{t=1}^{T}\sum_{s=1}^{N_s}\left[C_{s,t}^k + C_{ps,t}^k + C_{rs,t}^k\right] \tag{17}$$

The solar direct cost (18), penalty cost (19) and reserve cost (20) can be expressed as:

$$C_{s,t}^k = K_s \times P_{s,t}^k \tag{18}$$

$$C_{ps,t}^k = K_{ps} \times \left(P_{s,av} - P_{s,t}^k\right) = K_{ps}\int_{P_{s,t}^k}^{P_{sr}}\left(p_{s,t}^k - P_{s,t}^k\right) f_s\left(p_{s,t}^k\right) dp_{s,t}^k \tag{19}$$

$$C_{rs,t}^k = K_{rs} \times \left(P_{s,t}^k - P_{s,av}\right) = K_{rs}\int_{0}^{P_{s,t}^k}\left(P_{s,t}^k - p_{s,t}^k\right) f_s\left(p_{s,t}^k\right) dp_{s,t}^k \tag{20}$$

Where $f_s\left(p_{s,t}^k\right)$ is the PDF of solar power at time t; $P_{s,av}$ is the available solar generation; K_s, K_{ps} and K_{rs} are the direct solar, penalty, reserve cost coefficients for s[th]solar power plant;

2.6.3 Battery-storagecost (BC) model

In this model, we assume that battery cost is independent of power draw (P_b) but dependent on energy storage level ($SOC_{b,t}^k$) [37] with the total number of batteries N_{batt} as given in (21).

$$BC = H_b(SOC_{b,t}^k) = \sum_{t=1}^{T}\sum_{b=1}^{N_{batt}} h_b\left(SOC_{b\max} - SOC_{b,t}^k\right) \tag{21}$$

Where $SOC_{b\max}$ is the maximum storage capacity of a battery and h_b imposes a penalty proportional to the stored energy level's deviation from the unit capacity on the battery's cost function.

2.6.4 **Consumer-benefitcost (CC) model**

This model represents the benefit cost, which is obtained from the benefit-cost curve as a function of real power consumption as given in (22).Here, the load is treated as price-based demand, and social welfare (SW) is defined as consumer benefit costs minus producer costs. Moreover, these consumer benefit costs are treated as negative costs into an objective function. Thus, there would be an increase in social welfare or a reduction in the expected total cost [9].

$$CC = B_{L_i}(P_{L_i,t}^k) = \sum_{t=1}^{T}\sum_{i=1}^{N_L} a_{L_i}\left(P_{L_i,t}^k\right)^2 + b_{L_i}P_{L_i,t}^k + c_{L_i} \tag{22}$$

Where a_{L_i}, b_{L_i} and c_{L_i} are the coefficients of thebenefit-cost functions; N_L is the total number of load buses; $P_{L_i,t}^k$ is theload demand power.

2.7 Constraints

2.7.1 AC power flow constraints

The real and reactive power balance equations are given as follows:

$$\left.\begin{aligned} P_{i,t}^k &= P_{G_i,t}^k + P_{s,t}^k - P_{ch_b,t}^k + P_{dch_b,t}^k - P_{L_i,t}^k \\ Q_{i,t}^k &= Q_{G_i,t}^k - Q_{L_i,t}^k \end{aligned}\right\} \quad \forall i,s,b,k,\mathrm{t} \in \mathrm{T}, \tag{23}$$

The calculated real ($P_{i,t}^k$) and reactive ($Q_{i,t}^k$) powers at time (t) are given as:

$$\left.\begin{aligned} \mathrm{P}_{i,t}^{k} &= \mathrm{V}_{i,t}^{k} \sum_{j=1}^{N_{bus}} \mathrm{V}_{j,t}^{k} \left[G_{ij} \cos\left(\theta_{ij,t}^{k}\right) + B_{ij} \sin\left(\theta_{ij,t}^{k}\right) \right] \\ Q_{i,t}^{k} &= \mathrm{V}_{i,t}^{k} \sum_{j=1}^{N_{bus}} \mathrm{V}_{j,t}^{k} \left[G_{ij} \sin\left(\theta_{ij,t}^{k}\right) - B_{ij} \cos\left(\theta_{ij,t}^{k}\right) \right] \end{aligned}\right\} \mathrm{i} \in \mathrm{N}_{\mathrm{bus}} \tag{24}$$

Where $Q_{G_i,t}^{k}$ and $Q_{L_i,t}^{k}$ are the i^{th} reactive power output and reactive load demand in MVAR; voltage magnitude and difference in phase angle are $V_{i,t}^{k}$ and $\theta_{ij,t}^{k} = \theta_{i,t}^{k} - \theta_{j,t}^{k}$; G_{ij} and B_{ij} are the conductance and susceptance between buses i and j, respectively; $\mathrm{N_{bus}}$ is the total number of buses.

Thermal generator boundary limits: The active power and reactive power generation limits, and also generator voltage limits are given as [4]:

$$\left.\begin{aligned} P_{G_i}^{\min} &\le P_{G_i,t}^{k} \le P_{G_i}^{\max} \\ Q_{G_i}^{\min} &\le Q_{G_i,t}^{k} \le Q_{G_i}^{\max} \\ V_{G_i}^{\min} &\le V_{G_i,t}^{k} \le V_{G_i}^{\max} \end{aligned}\right\}, \forall\, i \in \left\{1, 2, 3, \ldots N_G\right\} \tag{25}$$

BESS constraints: The battery storage limits, charging, anddischarging power limits are given as:

$$\left.\begin{aligned} SOC_b^{\min} &\le SOC_{b,t}^{k} \le SOC_b^{\max} \\ P_{ch_b}^{\min} &\le P_{ch_b,t}^{k} \le P_{ch_b}^{\max} \\ P_{dch_b}^{\min} &\le P_{dch_b,t}^{k} \le P_{dch_b}^{\max} \end{aligned}\right\}, b \in N_{batt}, t \in T \tag{26}$$

Solar power constraints:

$$0 \le \mathrm{P}_{\mathrm{s,t}}^{\mathrm{k}} \le \mathrm{P}_{\mathrm{s_{max}}}^{\mathrm{k}}, \forall\ \mathrm{s} \in \left\{1, \ldots\ldots \mathrm{N_s}\right\} \tag{27}$$

Transformer taps setting constraints:

$$\mathrm{k}_{\mathrm{A\,min}}^{\mathrm{k}} \le \mathrm{k}_{\mathrm{A,t}}^{\mathrm{k}} \le \mathrm{k}_{\mathrm{A\,max}}^{\mathrm{k}}, \forall \mathrm{A} \in \left\{1, \ldots\ldots \mathrm{N_{rt}}\right\} \tag{28}$$

Where $\mathrm{N_{rt}}$ is the total number of regulating transformers

Reactive power injections constraints:

$$\mathrm{Q}_{\mathrm{c_{min}}}^{\mathrm{k}} \le \mathrm{Q}_{\mathrm{c,t}}^{\mathrm{k}} \le \mathrm{Q}_{\mathrm{c_{max}}}^{\mathrm{k}}, \forall \mathrm{c} \in \left\{1, \ldots\ldots \mathrm{N_{cap}}\right\} \tag{29}$$

where $\mathrm{N_{cap}}$ is the total number of shunt capacitors.

Security Constraints: Load bus voltages and transmission line loadings are examples of these constraints, which can be stated as,

$$\left.\begin{aligned} \mathrm{V}_{\mathrm{L_{min}}}^{\mathrm{k}} &\le \mathrm{V}_{\mathrm{L,t}}^{\mathrm{k}} \le \mathrm{V}_{\mathrm{L_{max}}}^{\mathrm{k}}, \forall \mathrm{L} \in \left\{1, 2, 3, \ldots\ldots \mathrm{N_L}\right\} \\ \mathrm{S}_{\mathrm{l,t}}^{\mathrm{k}} &\le \mathrm{S}_{\mathrm{l_{max}}}, \forall \mathrm{l} \in \left\{1, 2, 3, \ldots\ldots \mathrm{N_{trl}}\right\} \end{aligned}\right\} \tag{30}$$

where $\mathrm{N_{trl}}$denotes the total number of transmission lines.

Ramp-up and down limits of generating limits: The ramp up and down limits are given as:

$$\left.\begin{aligned} P_{G_i,t+1}^{\max} &= min\left(P_{G_i}^{\max}, P_{G_i,t}^{k} + RU_i\right) \\ P_{G_i,t+1}^{\min} &= max\left(P_{G_i}^{\min}, P_{G_i,t}^{k} - RD_i\right) \end{aligned}\right\} \tag{31}$$

where $\mathrm{RU_i}$ and $\mathrm{RD_i}$ are the up and down ramp rate limits of i^{th} generating unit in MW per hour respectively.

Prohibited zones operating limits: In prohibited areas, generating unit operation is usually avoided are as follows [4]:

$$P_{G_i,t}^k \in \begin{cases} P_{Gi}^{\min} \le P_{G_i,t}^k \le P_{i,1}^L & \text{or} \\ P_{i,n_z-1}^U \le P_{G_i,t}^k \le P_{i,n_z}^L & \text{or} \\ P_{i,n_{pz}}^U \le P_{G_i,t}^k \le P_{G_i}^{\max} & n_z = 2,3,....,n_{pz} \end{cases} \tag{32}$$

where n_z is the index of prohibited zones in the i[th] generating unit, the number of prohibited operating zones in the i[th] generating unit is expressed by n_{pz}; $P_{i,n}^L$ and $P_{i,n}^U$ are the upper and lower boundaries of i[th] unit, n_z[th] prohibited operating zone in MW.

Voltage Stability Index [58]:

$$L_{l,t}^k \le L_{l,\max}, \forall l \in \{1,\ldots\ldots N_{trl}\} \tag{33}$$

2.7.2 AC-DC Power Flow

In existing HVDC-link into the AC system, the converter terminal AC buses mismatch equations are modified as [48]:

$$\left.\begin{aligned} P_{i,t}^k &= P_{G_i,t} + P_{s,t}^k - P_{ch_b,t}^k + P_{dch_b,t}^k - P_{L_i,t}^k - V_{D_y,t}^k I_{D_y,t}^k sign(y) \\ Q_{i,t}^k &= Q_{G_i,t} - Q_{L,t} - V_{D_y,t}^k I_{D_y,t}^k \tan\left(\varphi_{D_y,t}^k\right) \end{aligned}\right\} \tag{34}$$

On the DC side, where Nc is the number of converter buses,the DC voltage, current and power factor angle are $V_{D_y,t}^k$, $I_{D_y,t}^k$ and $\varphi_{D_y,t}^k$ respectively. The converter would act either as a rectifier (R) or an inverter (I) depending on whether sign convention ($sign(y)$) is +1 or -1.

2.7.3 DC system constraints

Generally, DC system model equations contain converter voltages, DC network equations and control equations such as specified DC voltage, firing angle can be summarised as follows [48]:

$$\left.\begin{aligned} & V_{D_y,t}^k - k_{D_y,t}^k V_{i,t}^k \cos\phi_{D_y,t}^k + X_{c_y} I_{D_y,t}^k = 0 \\ & V_{D_y,t}^k - k_\gamma k_{D_y,t}^k V_{i,t}^k \cos\varphi_{D_y,t}^k = 0 \\ & sign(y) I_{D_y,t}^k - \sum_{j=1}^{n_c} g_{D_y j} V_{D_y,t}^k = 0 \\ & V_{D_y,t}^k - V_{D_y}^{min} = 0 \\ & \cos\phi_{D_y,t}^k - \cos\phi_{D_y}^{min} = 0 \end{aligned}\right\} \forall y \in N_c \tag{35}$$

Where, $k_{D_y,t}^k$ is the converter transformer ratio; $\phi_{D_y,t}^k$ is the rectifier's angle with α_y firing angle; $\phi_{D_y,t}^k$ is the inverter's angle with γ_y extinction angle; X_{c_y} is the commutation reactance; k_γ is constant and is equal to 0.995 [48]; $g_{D_{yj},t}$ is the elements of DC nodes conductance matrix, respectively.

DC network constraints: The maximum and minimum limits of DC network variables are as follows:

$$\left.\begin{aligned} V_{D_y}^{\min} \le V_{D_y,t}^k \le V_{D_y}^{\max} \\ k_{D_y}^{\min} \le k_{D_y,t}^k \le k_{D_y}^{\max} \\ \phi_{D_y}^{\min} \le \phi_{D_y,t}^k \le \phi_{D_y}^{\max} \end{aligned}\right\}, \forall y \in \{1,2,3\ldots\ldots N_c\} \tag{36}$$

3 Solution methodology

3.1 Standard differential evolution

Differential evolution (DE) [54] is a powerful population-based stochastic search algorithm that can solve a wide variety of optimization problems in a variety of real-world applications, including large-scale nonlinear, non-convex and non-differentiable problems. Because of its ease of deployment, reliability, robustness, and performance, it has been recognised as a popular global optimization. A population of N_{pop} individuals is generated at random at the start of the DE algorithm. Each individual represents a point in the search space and contributes to the fitness value by establishing a distinction between itself and the other population.

The major phases of the standard DE algorithm can be described as follows:

Initialization: Initialize all j^{th} individuals of i^{th} population (u_{ij}) randomly within the limits of the given constraints in the search-space.

$$u_{ij}^{\tau_0} = u_j^{min} + rand * (u_j^{max} - u_j^{min}) , \forall j = 1, 2.., M, \ \& \ i = 1, 2, .., N_{pop} \tag{37}$$

where M is the dimensionality of the problem; N_{pop} is the size of the total population; u_j^{min} and u_j^{max} are the lower and upper bounds of the jth individual;

Mutation: As a next phase, this operator is applied based on the scaled difference between two selected individuals in the standard DE in a continuous search space. The following equation expresses the most common mutation scheme used in DE:

$$mu_{ij}^{\tau+1} = u_{r_{1a}j}^{\tau} + F_s \times (u_{r_{2a}j}^{\tau} - u_{r_{3a}j}^{\tau}) \tag{38}$$

where F_s is referred to as the scaling factor in the [0, 1] range that governs the amplification of the differential variation $(u_{r_{2a}j}^{\tau} - u_{r_{3a}j}^{\tau})$, τ is the iteration times; $r_{1a}, r_{2a}, r_{3a} \in [1, \ N_{pop}]$ are integers which are chosen randomly.

Crossover: A crossover operation is introduced after the mutation phase to increase the population's diversity. The target vector is shuffled to generate the trial vector $(co_{ij}^{\tau+1})$ with the mutant vector $(mu_{ij}^{\tau+1})$. In crossover operations, the following scheme is used:

$$co_{ij}^{\tau+1} = \begin{cases} mu_{ij}^{\tau+1}; & (rand(j) \le CR) or (j = J) \\ u_{ij}^{\tau}; & Otherwise \end{cases} \tag{39}$$

where CR is the crossover rate, the range is (0,1). Jis an integer chosen at random from the range [1, M] and $rand(j)$ is a uniformly distributed stochastic number in the range of (0,1);

Selection: The selection operator in DE determines the survival of a trail vector $(co_{ij}^{\tau+1})$ or target vector (u_i^{τ}) and goes to the next iteration based on its objective values. The following equation is defined as a selection operator:

$$u_i^{\tau+1} = \begin{cases} co_i^{\tau+1}; & if \ \ f(co_i^{\tau+1}) \le f(u_i^{\tau}) \\ u_i^{\tau} \ ; & Otherwise \end{cases} \tag{40}$$

Where $f(.)$ is the key obj*e*ctive function to be min*i*mized (Total expected security cost).

3.2 Proposed modified DE (MDE) algorithm

Despite its widespread use in real-world applications, the standard DE suffers from avariety of over diversity issues caused by the random selection of dimensions, leading in poor solution quality and convergence performance for complex multimodal optimization problems [54–58]. On the other hand, using a large-scale population and a multi-population approach would significantly increase the computed amount while reducing the algorithm's convergence speed. Therefore, a modified DE (MDE) algorithm is proposed by introducing a new crossover and a new local control strategy for adjusting local variables, which are

combined to increase the DE's efficiency and effectiveness with a smaller population size [59]. As the evolution mechanism changes, the crossover rate (CR) changes as well. This is done to keep the power of exploration and the power of extraction in balance.The MDE alg*o*rithm, on the other hand, differs from the standard DE algorithm in three ways.

(1) Prior to mutation and crossover operation, each trail vector (co_i^{τ}) is allocated to a target vector (u_i^{τ}).

(2) To improve the capability of global search, a new local control approach is introduced into the crossoveroperator.

(3) The parameter CR is supervised for both mutation and crossover.

The next sub-sections 3.2.1, 3.2.2and 3.2.3 examine these differences.**Fig. 3** shows the proposed MDE algorithm in detail.

The dynamic crossover rate: In contrast to standard DE, where CR is fixed from start to end, the proposed NDE algorithm employs a dynamic CR function. CR achieves a high probability value for mutations, crossover, and local adaptation in the early stages of evolution. In the following step, CR has a low value for changing the decision parameters to obtain high - precision solutions.

The expression of CR is given as follows:

$$CR(\tau) = CR_{max} \cdot \left(\frac{CR_{min}}{CR_{max}}\right)^{\frac{\tau}{\tau_{max}}} \tag{41}$$

Where τ_{max} is the total number of iterations

The local adaptation approach: The local adaptation (LA) approach is proposed to prevent local search in the early stages of evolution while still using high-precision solutions later on. This approach is based on step-disturbance and random-perturbation. Using the local adaptation rate (LAR), a trial solution can bealtered in the vicinity of the current location with the help of the step-disturbance. Also, random-perturbation is used to explore new unknown regions in the feasible space with *a probability* of 0.1 LAR, mainly to prevent trapping in local search.

$$LAR(\tau) = LAR_{min} \cdot \left(\frac{LAR_{max}}{LAR_{min}}\right)^{\frac{\tau}{\tau_{max}}} \tag{42}$$

The adaptation step (AS) differs dynamically with the τ - iteration as shown in (43). The AS with a high value aims at exploring new areas in the initial process of evolution. As the value of τ increases, AS decreases steadily from AS_{max} to AS_{mid}. When there is also a very small AS value for the region including an ideal global solution, the DE will start focusing all efforts on the use of the high-precision solution in the discovered region.

$$AS(\tau) = \begin{cases} AS_{max} \cdot \left(\frac{AS_{mid}}{AS_{max}}\right)^{\frac{\tau}{\tau_{max}/2}}, & \tau \le \frac{\tau_{max}}{2} \\ AS_{mid} \cdot \left(\frac{AS_{min}}{AS_{mid}}\right)^{\frac{\tau - \tau_{max}/2}{\tau_{max}/2}}, & \tau > \frac{\tau_{max}}{2} \end{cases} \tag{43}$$

Where $AS_{min} < AS_{mid} < AS_{max}$

Integrating the mutation and crossover operations: In the standard DE, whether the crossover operation is carried out on $\left(u_{ij}^{\tau}\right)$ or not, the mutation operation is always performed on each variable $\left(u_{ij}^{\tau}\right)$ of target vector $\left(u_i^{\tau}\right)$ so as to generate the donor vector $\left(mu_{ij}^{\tau}\right)$. However, usually, there are only part of values in $\left(mu_{ij}^{\tau}\right)$ could be adopted in trial vector $\left(co_{ij}^{\tau}\right)$, which is as follows

$$co_{ij}^{\tau+1} = \begin{cases} mu_{ij}^{\tau+1}; & \left(rand(j) \le CR\right) or \left(j = J\right) \\ u_{ij}^{\tau}; & Otherwise \end{cases} \tag{44}$$

For a high-dimensional problem, if the value of CR (τ) is very small, the mutation operation is only applied to a few variables, resulting in a lot of redundant computations. To remove redundant calculations, the proposed MDE algorithm combines the mutation and crossover operations, with the mutation operation being performed only on the individuals chosen for the crossover operation.

3.3 Constraints repairing mechanism in ESCDOPF problem

In evolutionary computation optimization algorithms, there are many ways to tackle constraints. The methods for repairing constraints described below are the most widely used. They are the feasible solution preservation method, the infeasible solution denial method, the penalty function method, and the solution repair method. The penalty function method is the most widely used of all the methods [58]. In this paper, the penalty function method is handled by integrating all the inequality constraints into the fitness function. In this procedure, the objective function is multiplied by a penalty factor equal to the square of the variable's violated value, and any infeasible solution obtained is rejected.
Therefore, the extended objective function is augmented with the inequality constraints and is given by:

$$\begin{aligned} ESC = {} & GC + SC + BC + CC + \lambda_P * \sum_{t=1}^{T}\sum_{i=1}^{N_G}\left(P_{G_i,t} - P_{G_i}^{\lim}\right)^2 + \lambda_{PV} * \sum_{t=1}^{T}\sum_{s=1}^{N_s}\left(P_{s,t} - P_s^{\lim}\right)^2 \\ & + \lambda_Q * \sum_{t=1}^{T}\sum_{i=1}^{N_G}\left(Q_{G_i,t} - Q_{G_i}^{\lim}\right)^2 + \lambda_V * \sum_{t=1}^{T}\sum_{L=1}^{N_L}\left(V_{L,t} - V_L^{\lim}\right)^2 + \lambda_S * \sum_{t=1}^{T}\sum_{l=1}^{N_{trl}}\left(S_{l,t} - S_l^{\max}\right)^2 \\ & + \lambda_L * \sum_{t=1}^{T}\sum_{L=1}^{N_L}\left(L_{L,t} - L_L^{\lim}\right)^2 + \lambda_b * \sum_{t=1}^{T}\sum_{b=1}^{N_{batt}}\left(SOC_{b,t} - SOC_b^{\lim}\right)^2 + \lambda_{VD} * \sum_{t=2}^{T}\sum_{y=1}^{N_C}\left(V_{D_y,t} - V_{D_y}^{\lim}\right)^2 \\ & + \lambda_{TD} * \sum_{t=1}^{T}\sum_{y=1}^{N_C}\left(k_{D_y,t} - k_{D_y}^{\lim}\right)^2 + \lambda_{AD} * \sum_{t=1}^{T}\sum_{y=1}^{N_C}\left(\phi_{D_y,t} - \phi_{D_y}^{\lim}\right)^2 \end{aligned} \tag{45}$$

where the penalty factors for ramp-rate limits, solar power limits, reactive power limits, voltage limits, line-loading limits, line voltage stability limits, battery storage limits, dc voltage limits, converter transformer ratio limits, trigger angle or extinction angle limits are λ_P, λ_{PV}, λ_Q, λ_V, λ_S, λ_L, λ_b, λ_{VD}, λ_{TD} and λ_{AD}. The limit value of the dependent variable u is $u^{\lim}$ is provided as:

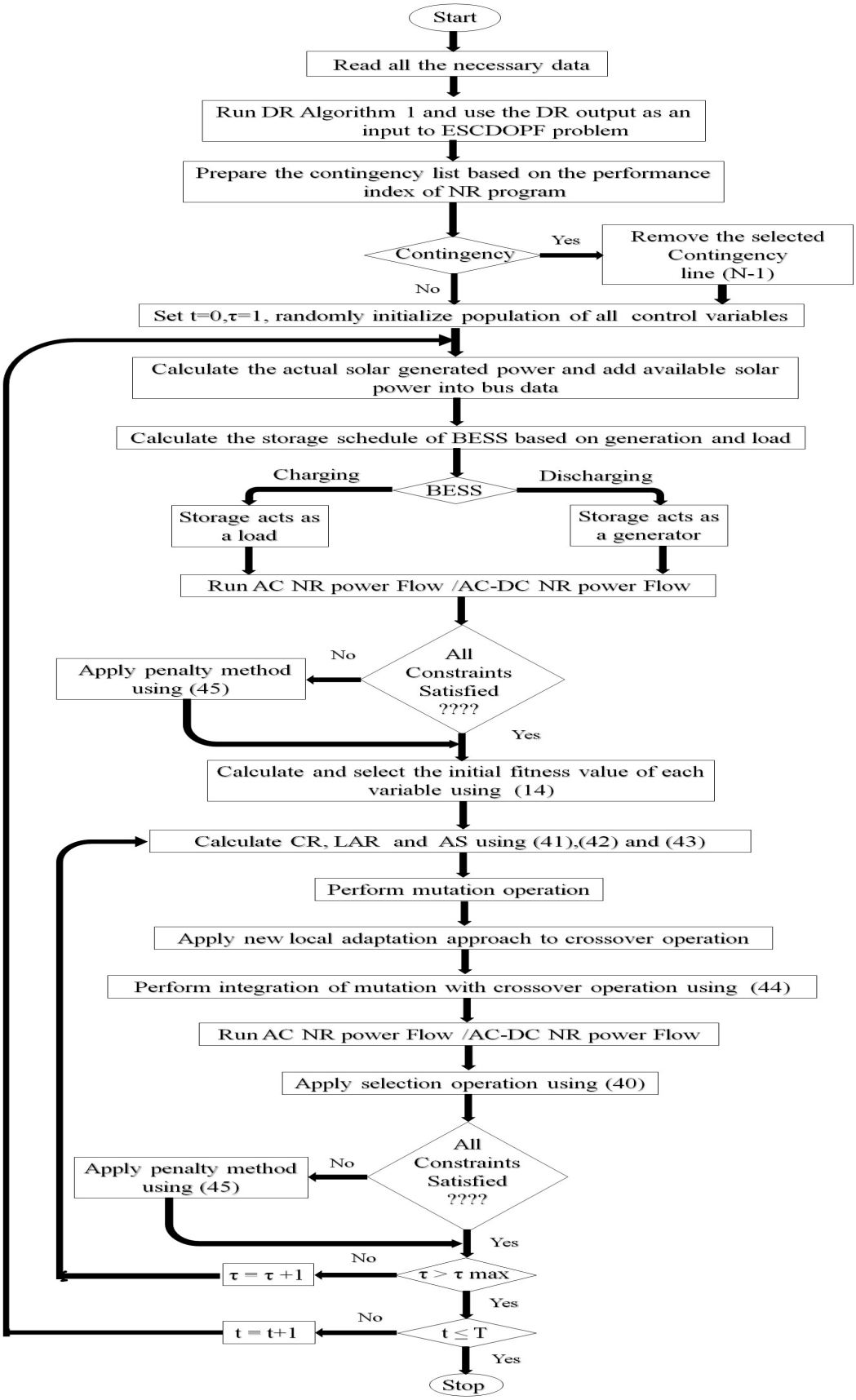

Fig. 3 Proposed MDE algorithm to solve ESCDOPF problem

$$u^{lim} = \begin{cases} u_{max} & u > u_{max} \\ u_{min} & u > u_{max} \end{cases} \quad (46)$$

4 Test system data

4.1 DR system data

In general, the interconnected power system includes all types of demand (residential, industrial, and commercial). However, in this paper, 10% of the total load is considered as residential consumers. There are several controllable appliances for each consumer which may include PHEVs, dishwashers, water heaters, kettles, washing machines, and other appliances. For this study, each residential consumer is selected to have four controllable appliances which are divided equally among them. As compared to commercial and industrial zones, these controllable appliances can be effectively handled during the load shifting operation. Therefore, the game theory-based energy scheduling problem of the controllable appliances is applied to residential consumers.

Based on the per day schedule of a consumer, the average energy consumption value is considered as 25 kWh. The operating specifications of the controllable appliances are depicted in **Appendix A1**. Unless stated otherwise, the price parameters are fixed according to the DAP scheme with two periods i.e., critical peak load period and low off-peak load period prices as 10 $/MWh and 5 $/MWh respectively.

5 Simulation results and discussions

In this paper, the proposed MDE algorithm-based ESCDOPF with solar and FRs such as DR, BESS, and HVDC systems has been evaluated on an IEEE-30 bus system, to validate its potential. All numerical studies have been run on an Intel Core i5 processor, 4 GB of RAM, and the program is coded in MATLAB. In implementing the proposed algorithm, the modified DE control parameters data are given in **Appendix A2**.

5.1 Conventional IEEE 30 bus system on the DOPF model

In this paper, the complete IEEE 30 bus system data along with generator fuel cost, consumer benefit cost, forecasted load demand ramp rate limits and all other data are taken from [4, 60]. To compare the outcomes of the proposed MDE algorithm with other existing heuristic algorithms, we first addressed the DOPF problem that have been solved in prior works. This enables us to compare our findings with the existing literature to better illustrate the effectiveness of the proposed MDE approach. This research then solves the ESCDOPF problem for different scenarios and different case studies with the MDE algorithm. The results are then compared to those from other case studies developed for each scenario in this study.

Furthermore, pertaining to the DOPF problem with Eq. (16) as an objective function. The total fuel-cost comparison results of the proposed MDE, DE and other heuristic algorithms are presented in **Table 1**. It can be observed that the proposed MDE has given a better outcome with less computational cost and less population size. It is evident from **Fig. 4**, that the proposed MDE outperforms the standard DE with 30,40 and 50 different population sizes in terms of obtaining the best value of fuel cost of 16,496 $/day over 500 iterations. **Fig. 4** also reveals that the DE algorithm at population size (Npop=30) are stuck at local optimum with high convergence rate, whereas at population sizes (Npop=40 and 50), the DE reaches the near optimal solution with a lower convergence rate. Due to the dynamic crossover rate (DCR) and local control strategy, the proposed MDE algorithm is efficient and robust compared to the DE algorithm in terms of obtaining a precise solution and faster convergence with a smaller population size (i.e., Npop=5).

Table 1 DOPF: Obtained results with MDE and other algorithms

Method	Fuel Cost ($/day)	Time (sec)
SA [4]	16,703.81	1408.46
PSO [4]	16,619.92	811.69
DE (Npop=30)	16,522.99	392.02
DE (Npop=40)	16,509.34	533.35
DE (Npop=50)	16,505.82	666.95
MDE (proposed)	**16,496.00**	**128.06**

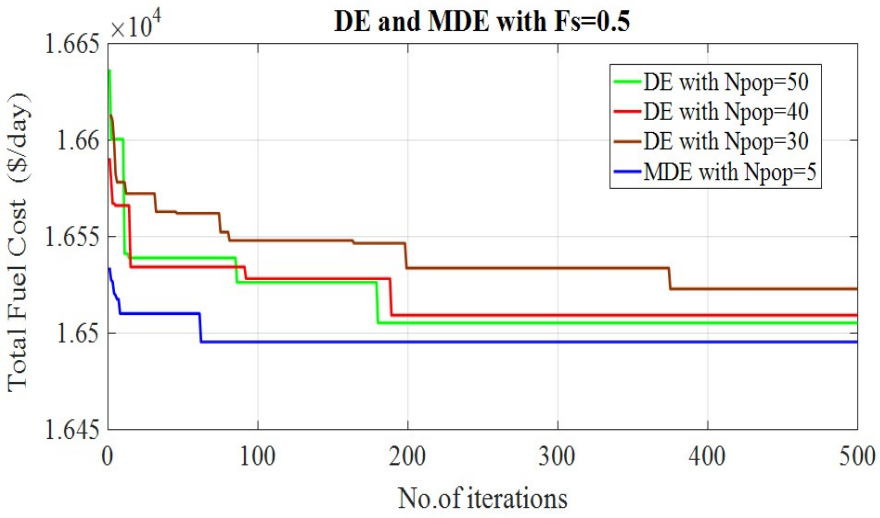

Fig. 4 DOPF fuel cost convergence characteristics

5.2 Modified IEEE 30 bus system on the ESCDOPF model

In this system, the modified IEEE 30 bus system is used to accommodate solar power plants, with a total capacity of 20 MW is located at bus 24, which is considered arbitrarily. The solar irradiance information with hourly resolution is accessible on the National Renewable Energy Laboratory (NREL) webpage [61]. The parameters of the Beta distribution are estimated at 2.9721 and 8.9928 as scale factor (a_s) and shape factor (b_s).Therefore, the actual forecasted solar power ($P_{s,act}$) is plotted in **Fig. 5.** In order to obtain solar power generation ($P_{s,t}^{k}$), it is assumed that solar forecast is affected by an appropriate error. So, as a random variable the maximum solar power fluctuation is considered as 20% of the forecasted value. Then the solar power is considered to be schedulable. The cost-coefficients of solar generators are K_s =9 Rs/MWh, K_{ps} = 1.5 Rs/MWh, and K_{rs} = 11 Rs/MWh respectively. Additionally, on bus 14, a 100 MWh BESS with a battery SOC that can range from 40% to 100% of the rated battery capacity is installed. Both the charging and discharging efficiencies of η_{ch_b} and η_{dch_b} are set to 90%. The battery power limits are set to $0 \le P_b \le 20$ MW. The h_b is assumed to be 1.0 Rs/MWh.

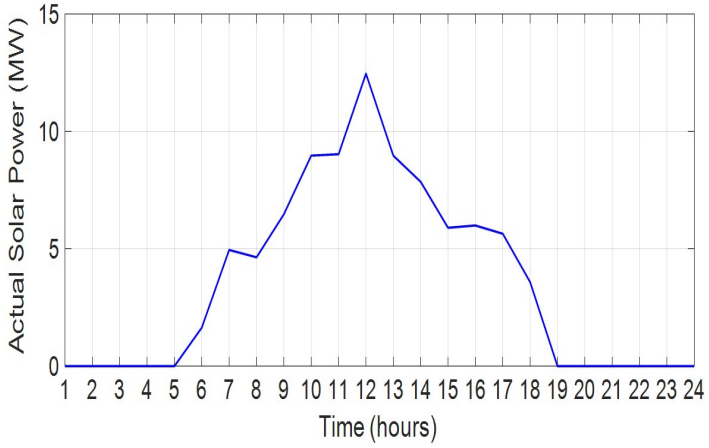

Fig. 5 Actual forecasted solar power generation

The proposed MDE algorithm is tested for both normal and post-contingency states.To study the performance of the proposed MDE, two scenarios are considered as below:

5.2.1Scenario-A) Performance of solar with and without FRs during normal and post-contingency states (without HVDC link)
5.2.2. Scenario-B) Performance of solar with and without FRs during normal and post-contingency states (with TTHVDC links)

To investigate the performance solar and without/with FR on the operation of the proposed MDE based ESCDOPF model in all scenarios, different cases are considered for each scenario, as given below.

(i) Case 0: Base case (with solar and all FR are ignored)
(ii) Case 1: With solar + with 5% DR
(iii) Case 2: With solar + with 10% DR
(iv) Case 3: Withsolar + with 0% DR +with BESS
(v) Case 4: Withsolar + with 5% DR + with BESS
(vi) Case 5: With solar + with 10% DR + with BESS

The proposed method for modified IEEE 30 bus system is solved with solarand without BESS and DR for the selected forecasted load profile data was discussed in case 0 (base case). Moreover, without BESS and with solarand DR having 5% and 10% participation levels are considered in cases 1 and 2. Further case studies are solved with solarand BESS under 0%, 5% and 10% participation levels of DR.

5.2.1 Scenario-A

This scenario examines the effect of solar with and without FR on the ESCDOPF of the proposed algorithm without considering the HVDC link.

(i) DR effect on the utility side:

First, before the activation of schedulers embedded in the smart meters, the actual hourly forecasted load demand has been given as an input to the game theory-based DR, in which it is separately tested for the ESCDOPF model. Note that the sum of the total energy demand over all 24 hours during 0%, 5% and 10% DR implementation is the same and is equal to 5731.56 MWh. This demonstrates that without altering the total amount of consumption, the DR approach can shift the load. This may be important for the comfort of end-users. The load demand profile before and after applying the DR with 5%and 10% PLs is shown in **Fig. 6.** One can observe from **Fig. 6**that after the implementation of DR, the peak demand is reduced by 15.4 MW/day and 30.8 MW/day with 5 % and 10% PLs, respectively. As a result, the per day utility energy bill savings increased by $430 and $860 respectively. In this way, the utility firm receives more benefits as the DR PLs increase.

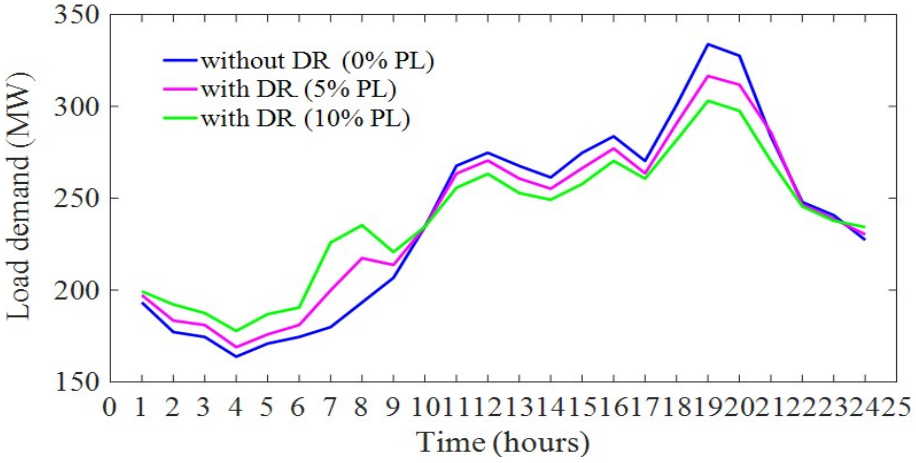

Fig. 6 Load demand profiles of 30 bus system without and with DR

(ii) Solar and FR effect on the generation side

From **Fig. 6**, the actual forecasted load (i.e., 0% PL) is considered, the peak load hours have chosen at 18:00-20:00 hours, after DR implementation with 5% and 10% PLs, thepeak load hours are chosen at 19:00-20:00 hours and 19:00 hour respectively. The storage schedules are determined based on the generation limits of all the generators and load demand. By proper selection of charging and discharging hours, the BESS would act either as a variable load or a generator, depending on whether to absorb surplus active power or to provide deficit active power. When the BESS is used after DR, the total charging power is greater than the total discharging power. Due to this, there is a reduced peak load of power. Because of reduced peak load power, the size of system equipment, and the reserve capacity of the system are reduced.
Furthermore, single transmission line outage was used to include a contingency in this simulation. Using bus 1 as a reference, 36 "N-1" contingencies are defined in which islanding circuits are excluded. In this work, the performance index (PI) is measured by the Newton- Raphson load flow (NRLF) approach, was used to rank the contingencies [25]. Following a security review, it was discovered that the outage of the line connecting buses 6–8 creates the network's most severe contingency situation. The proposed MDE is implemented to solve ESCDOPF problem of taking preventive control measures like generator rescheduling and load shifting without considering generator ramping costs and load interruption costs, in order to return the

system to its original state while satisfying model constraints. Moreover, SOC of BESS along the operational time frame is included in the ESCDOPF during normal and post-contingency states as shown in **Fig. 7**. This shows that the BESSs charge during the system's off-peak phase and discharge during the system's peak period, thus smoothing the load curve of the system. **Table 2** summarises the comparative cost findings of all cases with power losses and computational times in Scenario-A under normal and post-contingency states. The results demonstrate that the BESS and DR assist generating companies in lowering their fuel costs. The simulation findings indicate that higher DR participation levels resulted in a greater reduction in the value of the generation fuel cost. Nonetheless, by observing the total security costs (TSC) in **Table 2**, a reduction is observed in most cases. However, TSC is not as reduced in cases 3 and 4 as compared to previous cases. This is expected due to the inclusion of battery storage costs with low (0% and 5%) DR.

Table 2 Scenario-A: All cases cost findings with power losses and computational times under normal (N) and post-contingency(PC) states

(A) CASES		Solar Cost			Fuel Cost ($/day)	Consumer-Benefit Cost ($/day)	Battery-Storage Cost ($/day)	Total Security Cost ($/day)	Power Loss (MW/day)	Time (sec)
		Direct Cost ($/day)	Penalty Cost ($/day)	Reserve Cost ($/day)						
0	N	734.13	10.80	31.25	16188.00	100960.00	x	-83995.82	179.36	86.09
	PC	695.13	10.91	25.09	16209.00	100960.00	x	-84019.87	182.72	83.49
1	N	733.76	9.26	27.33	16129.00	102000.00	x	-85100.65	180.19	83.24
	PC	697.00	11.58	25.57	16137.00	102000.00	x	-85128.85	183.07	81.65
2	N	752.32	9.44	28.99	16069.00	103380.00	x	-86520.24	181.55	84.81
	PC	708.34	10.74	27.43	16095.00	103380.00	x	-86538.49	183.92	81.77
3	N	692.95	10.00	26.08	16114.00	100960.00	576.50	-83540.47	173.23	87.20
	PC	767.66	13.21	29.07	16081.00	100960.00	607.29	-83461.77	176.77	86.29
4	N	731.09	10.94	26.61	16047.00	102000.00	579.94	-84604.43	173.96	90.01
	PC	766.17	13.80	30.14	16030.00	102000.00	585.07	-84590.82	177.03	89.86
5	N	745.42	12.38	33.37	16000.00	103380.00	578.34	-86008.50	174.08	87.92
	PC	752.05	10.61	35.18	15944.00	103380.00	592.00	-86041.16	177.84	85.24

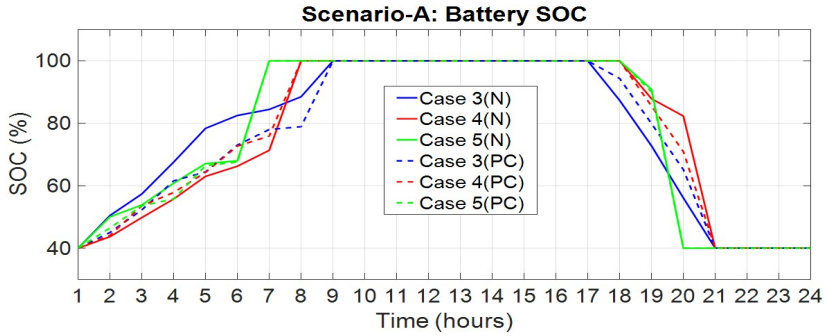

Fig. 7 Scenario-A:Battery SOC

5.2.2 Scenario-B

This scenario considers a TT-HVDC in extension with the existing proposed method (i.e., Scenario-A). The DC data for the TT-HVDC link that connects between 2 and 4 can be found in [46]. As noted previously and illustrated in **Fig. 8**, the BESS operation has a large impact on the total security cost and its SOC conditions during normal and post-contingency states, respectively. The DC control parameters solution values and powers at the converters are given in **Table 3**. The results obtained from the TT-HVDC link show that the proposed MDE approach enables the study of the effects of DC on the AC power flows during pre- and post-contingency states. This observation is delineated in **Table 4** forall the cases with their power losses and computational times**.**

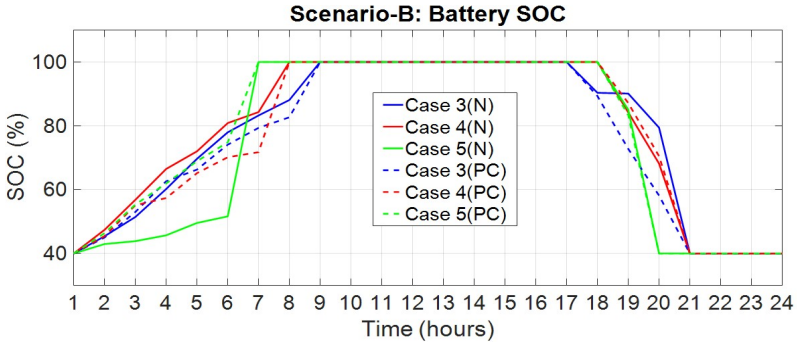

Fig. 8 Scenario-B: Battery SOC

Table 3 TT-HVDC-link control parameters values and their powers at the converters (case 0)

TT-HVDC Final values	V_{DR} (p.u)	k_{DR}	α_R (deg)	V_{DI} (p.u)	k_{DI}	γ_I (deg)	P_{DR} (MW)	Q_{DR} (MVAR)	P_{DI} (MW)	Q_{DI} (MVAR)	I_D (pu)
L 2-4	1.2962	0.988	8	1.29	1.008	16.5	59.109	37.907	58.824	37.242	0.456

Table 4 Scenario-B: All cases cost findings with power losses and computational times under normal (N) and post-contingency(PC) states

(B) CASES		Solar Cost			Fuel Cost ($/day)	Consumer-Benefit Cost ($/day)	Battery-Storage Cost ($/day)	Total Security Cost ($/day)	Power Loss (MW/day)	Time (sec)
		Direct Cost ($/day)	Penalty Cost ($/day)	Reserve Cost ($/day)						
0	N	733.74	10.87	25.09	16049.00	100960.00	x	-84141.29	168.03	108.41
	PC	723.75	11.13	26.45	16093.00	100960.00	x	-84105.66	171.85	106.41
1	N	738.73	9.99	29.24	15965.00	102000.00	x	-85257.02	169.32	103.17
	PC	733.20	10.2	31.85	16033.00	102000.00	x	-85191.74	171.98	102.08
2	N	730.31	10.92	26.76	15920.00	103380.00	x	-86704.00	170.09	114.51
	PC	715.78	12.38	25.83	15980.00	103380.00	x	-86646.00	172.08	107.35
3	N	728.19	10.01	38.03	15995.00	100960.00	593.11	-83595.66	164.91	108.89
	PC	738.29	11.01	32.26	15967.00	100960.00	616.64	-83594.80	167.70	108.13
4	N	742.80	10.28	33.69	15914.00	102000.00	532.76	-84766.45	165.87	111.01
	PC	746.22	12.24	30.25	15883.00	102000.00	543.36	-84784.91	167.94	108.04
5	N	745.71	12.37	38.14	15898.00	103380.00	560.23	-86125.54	166.62	106.96
	PC	752.89	10.17	40.70	15846.00	103380.00	569.31	-86160.91	168.98	105.8

Finally, from all the scenarios, the comparison convergence characteristics of total security costs for all cases during normal and post-contingency states are shown in **Fig. 9.** Analyzing the results of the table of all scenarios, it is observed that in all the cases has got maximum benefits correspondingly the generation/operation costs are also reduced due to the incorporation of solar and flexible resources.

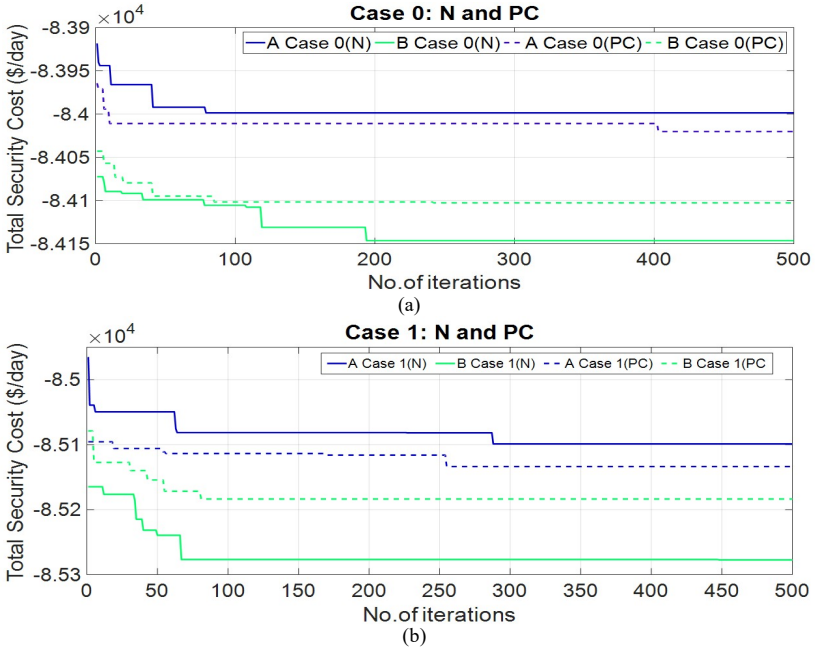

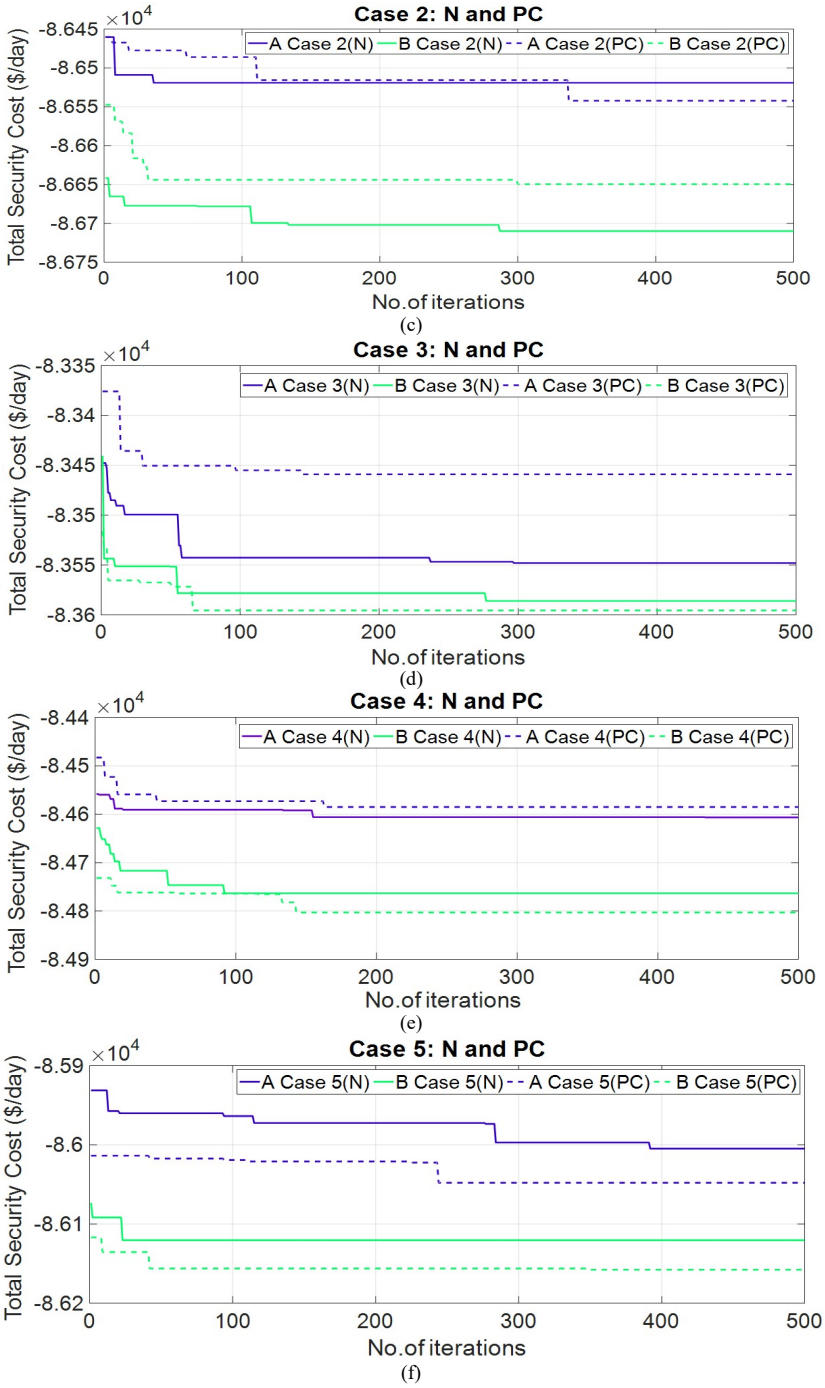

Fig. 9 Cost convergence characteristics curves of all scenarios A and B with all cases during normal and post contingency states (a) Case 0 (b) Case 1 (c) Case 2 (d) Case 3 (e) Case 4 (f) Case 5.

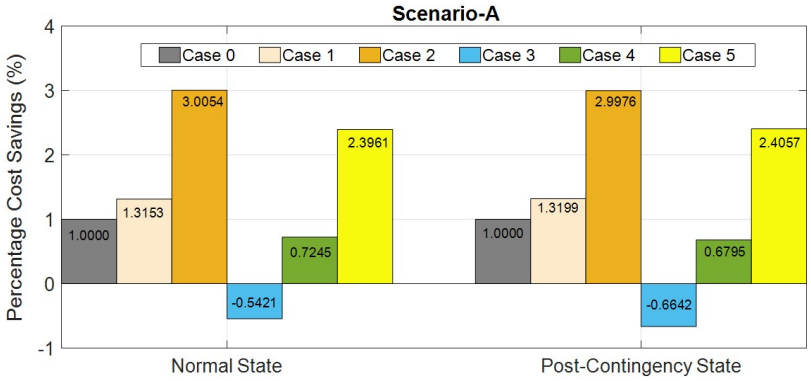

Fig. 10 Comparison of cost savings of all cases in Scenario-A

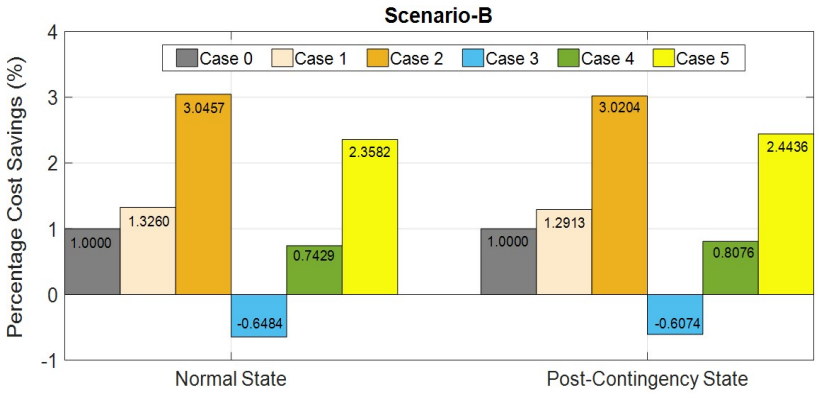

Fig. 11 Comparison of cost savings of all cases in Scenario-B

For Scenario-A, the percentage cost savings are observed for the respective cases during normal and post-contingency states, as given in **Fig. 10**. Likewise, for Scenario-B, the percentage cost savings are observed in all cases are shown in **Fig. 11**.Observing the percentage saving costs in **Fig. 10 and 11**, an increasing trend is observed in most cases. This is expected, due to the inclusion of battery storage cost with low (0%, 5%) DR.

6 Conclusions

This paper implements a new mathematical model of the ESCDOPF problem with solar and FR to enhance security and reliability while maximising utility and generation benefits. Moreover, the stochastic nature of solar causes uncertainties and variability which has a great impact on cost of operation. A game-theory based DR approach has been employed for handling the controllable loads and the minimisation of utility energy cost was considered as the objective. This study also confirms the idea that BESS is more useful not only for temporary energy shifts but also for reliability purposes. To enhance grid flexibility, TT LCC-HVDC systems are used as a fast-controlling device. To solve the ESCDOPF problem in the presence of solar and FRs, a modified DE (MDE) algorithm has been developed for minimising the objective function. Furthermore, the proposed MDE algorithm for the standard DOPF problem is compared to the standard DE and other existing algorithms to overcome the limitations of the standard DE approach, and a good result was reported with less convergence time and population size. The proposed MDE algorithm for theESCDOPF problem was evaluated in two scenariosin both normaland post-contingency states.According to the technical findings, the presence of solar and FRs provides significant benefits, such as reduced peak load, power losses, generation costs, and power consumption, as well as lower utility electricity bills. From the results, the proposed algorithm for the proposed model under consideration reduces total operation costs upto 3.0054 % in the test scenarios. A single-objective optimization problem is considered in this work. The MDE algorithm is also suitable to deal with multi-objective optimization problems, which is another interesting future scope.

Acknowledgements

This work is supported by the Ministry of electronics & information technology (MeitY), Government of India (GOI) through Visvesvaraya Ph.D. scheme under Grant MEITY-PHD-2352.
The authors are also thankful to the SERB, Government of India for providing infrastructure facilities under TARE research project (TAR/2018/000390).

References

[1] Doyle, C.; Loomans, L.; Truitt, A.; Lockhart, R.; Golden, M.; Dabbagh, K.; Lawrence, R. Solar Access to Public Capital (SAPC) Working Group: Best Practices in Commercial and Industrial (C&I) Solar Photovoltaic System Installation; Period of Performance. November 28, 2014–September 1, 2015.

[2] K. Morison, L. Wang and P. Kundur, "Power System Security Assessment", IEEE Power & Energy Magazine, pp. 30-39, Sept./Oct.2004.

[3] O. Alsac and B. Stott, "Optimal load flow with steady state security, IEEE Trans. Power App. Syst., vol. PAS-93, no. 3, pp. 745–751, Mar. 1974.

[4] T. Niknam, MR Narimani, M Jabbari, "Dynamic optimal power flow using hybrid particle swarm optimization and simulated annealing," Int. Trans. on Elec. Energy Systems 23 (7), 975-1001, 2013.

[5] Saber Armaghani, Nima Amjady, Oveis Abedinia, "Security constrained multi-period optimal power flow by a new enhanced artificial bee colony", Applied Soft Computing, vol. 37, Pages 382-395, 2015.

[6] F. Capitanescu, J.L. Martinez Ramos, P. Panciatici, D. Kirschen, A. Marano Marcolini, L. Platbrood, L. Wehenkel, State-of-the-art, challenges, and future trends in security constrained optimal power flow, Electric Power Systems Research, Volume 81, Issue 8, Pages 1731-1741, 2011.

[7] Y. Xu, Z. Y. Dong, R. Zhang, K. P. Wong and M. Lai, "Solving Preventive-Corrective SCOPF by a Hybrid Computational Strategy," in IEEE Trans. on Power Systems, vol. 29, no. 3, pp. 1345-1355, May 2014.

[8] Galvani, S., Talavat, V., & Rezaeian Marjani, S. "Preventive/Corrective Security Constrained Optimal Power Flow Using a Multi objective Genetic Algorithm". Elect. Power Comp. and Sys., 1–16, 2018.

[9] J. Condren, T. W. Gedra, and P. Damrongkulkamjorn, "Optimal power flow with expected security costs," IEEE Trans. Power Syst., vol. 21, no. 2, pp. 541–547, May 2006.

[10] J. Condren and T. W. Gedra, "Expected-security-cost optimal power flow with small-signal stability constraints," IEEE Trans. Power Syst., vol. 21, no. 4, pp. 1736–1743, Nov. 2006.

[11] R. S. Wibowo, N. Yorino, Y. Zoka, Y. Sasaki and M. Eghbal, "FACTS Allocation Based on Expected Security Cost by Means of Hybrid PSO," 2010 Asia-Pacific Power and Energy Engineering Conference, 2010, pp. 1-4, doi: 10.1109/APPEEC.2010.5448396.

[12] Qazi, A., Hussain, F., Rahim, N. A., Hardaker, G., Alghazzawi, D., Shaban, K., & Haruna, K. "Towards Sustainable Energy: A Systematic Review of Renewable Energy Sources, Technologies, and Public Opinions", IEEE Access, 7, 6383 63851, 2019. doi:10.1109/access.2019.2906402.

[13] ElDesouky A. "Security and stochastic economic dispatch of power system including wind and solar resources with environmental consideration". Int J Renew Energy Res, 2013;3(4):951–8.

[14] Surender Reddy, S., Bijwe, P. R., & Abhyankar, A. R. "Real-Time Economic Dispatch Considering Renewable Power Generation Variability and Uncertainty Over Scheduling Period". IEEE Systems Journal, 9(4), 1440–1451, 2015. doi:10.1109/jsyst.2014.2325967.

[15] Khan, N. A., Awan, A. B., Mahmood, A., Razzaq, S., Zafar, A., & Sidhu, G. A. S. "Combined emission economic dispatch of power system including solar photo voltaic generation". Energy Conversion and Management, 2015, vol 92, 82–91. doi: 10.1016/j.enconman.2014.12.02.

[16] Jadoun, V. K., Pandey, V. C., Gupta, N., Niazi, K. R., & Swarnkar, A. "Integration of renewable energy sources in dynamic economic load dispatch problem using an improved fireworks algorithm". IET Rene. Power Gen., 2018,12(9), 1004–1011.

[17] P. P. Biswas, P. N. Suganthan, and G. A. J. Amaratunga, ''Optimal power flow solutions incorporating stochastic wind and solar power,'' Energy Convers. Manage., vol. 148, pp. 1194–1207, Sep. 2017.

[18] Chamanbaz M, Dabbeney F, Lagoaz C, "AC optimal power flow in the presence of renewable sources and uncertain loads", IEEE Trans Power Syst, 1–22,2017.

[19] Kathiravan R, Kumudini Devi RP, "Optimal power flow model incorporating wind, solar, and bundled solar-thermal power in the restructured indian power system". Int J Green Energy, 2017, 14(11):934–950.

[20] Khan B, Singh P, "Optimal power flow techniques under characterization of conventional and renewable energy sources: a comprehensive analysis". J Eng Hindawi, 1–16, 2017.

[21] Syed, M.S., Chintalapudi, S.V., & Sirigiri, S. "Optimal Power Flow Solution in the Presence of Renewable Energy Sources". *Iranian Journal of Science and Technology, Transactions of Electrical Engineering, 45, 61-79,2020.*

[22] Tina, G., Gagliano, S., & Raiti, S. "Hybrid solar/wind power system probabilistic modelling for long-term performance assessment". Solar Energy,2006, 80(5), 578–588. doi: 10.1016/j.solener.2005.03.013.

[23] Ben Hmida, J., Javad Morshed, M., Lee, J., & Chambers, T. "Hybrid Imperialist Competitive and Grey Wolf Algorithm to Solve Multi-objective Optimal Power Flow with Wind and Solar Units". Energies, 11(11), 2891,2018. doi:10.3390/en11112891.

[24] Morshed, M.J.; Ben Hmida, J.; Fekih, A. "A probabilistic multi-objective approach for power flow optimization in hybrid wind-PV-PEV systems". Appl. Energy 2018, 211, 1136–1149,2018.

[25] Kiran Teeparthi, D.M. Vinod Kumar, "Multi-objective hybrid PSO-APO algorithm-based security constrained optimal power flowwith wind and thermal generators, Eng. Sci. and Tech., an Int. Journal, Volume 20, Issue 2, 2017, Pages 411- 426, ISSN 2215-0986, https://doi.org/10.1016/j.jestch.2017.03.002.

[26] H. Sharifzadeh, N. Amjady, and H. Zareipour, "Multi-period stochastic security-constrained OPF considering the uncertainty sources of wind power, load demand and equipment unavailability," Elect. Power Sys. Research, vol. 146, pp. 33–42, 2017.

[27] Teeparthi, K., Vinod Kumar, D.M., "Security-constrained optimal power flow with wind and thermal power generators using fuzzy adaptive artificial physics optimization algorithm". Neural Comput & Applic 29, 855-871, 2018.

[28] Akrami, A., Doostizadeh, M. & Aminifar, F. Power System flexibility: an overview of emergence to evolution. J. Mod. Power Syst. Clean Energy 7, 987-1007, 2019. https://doi.org/10.1007/s40565-019-0527-4.

[29] Mohsenian-Rad, V. W. S. Wong, J. Jatskevich, R. Schober and A. Leon-Garcia, "Autonomous Demand-Side Management Based on Game-Theoretic Energy Consumption Scheduling for the Future Smart Grid," in IEEE Transactions on Smart Grid, vol. 1, no. 3, pp. 320-331, Dec. 2010, DOI: 10.1109/TSG.2010.2089069.

[30] A. J. Conejo, J. M. Morales, and L. Baringo, "Real-time demand response model," *IEEE Trans. Smart Grid*, vol. 1, no. 3, pp. 236–242, Dec. 2010.

[31] P. Yang, G. Tang, and A. Nehorai, "A game-theoretic approach for optimal time-of-use electricity pricing," *IEEE Trans. Power Syst.*, vol. 28, no. 2, pp. 884–892, May 2013.

[32] H. Zhong, L. Xie, and Q. Xia, "Coupon incentive-based demand response: Theory and case study," *IEEE Trans. Power Syst.*, vol. 28, no. 2, pp. 1266–1276, May 2013.

[33] Jamshid Aghaei, Mohammad-Iman Alizadeh, Pierluigi Siano, Alireza Heidari, "Contribution of emergency demand response programs in power system reliability, Energy, Volume 103, 2016, Pages 688-696, https://doi.org/10.1016/j.energy.2016.03.031.

[34] B. Lokeshgupta and S. Sivasubramani, "Multi-objective dynamic economic and emission dispatch with demand side management," *Int. J. Elect. Power Energy Syst.*, vol. 97, pp. 334–343, 2018.

[35] Lokeshgupta Bhamidi & Sivasubramani Shanmugavelu," Multi-objective Harmony Search Algorithm for Dynamic Optimal Power Flow with Demand Side Management", Elec. Power Comp. and Sys., 47:8, 692-702, 2019.

[36] Suresh, V., Sreejith, S., Sudabattula, S. K., & Kamboj, V. K. "Demand response-integrated economic dispatch incorporating renewable energy sources using ameliorated dragonfly algorithm". Electrical Engineering,2019. doi:10.1007/s00202-019-00792-y.

[37] M. Chandy, S. Low, U. Topcu, and H. Xu, "A simple optimal power flow model with energy storage," Proc. of Conf. on Decision and control, pp. 1051-1057, 2010.

[38] Zhongwei Wang, Jin Zhong, Dong Chen, Yuefeng Lu and Kun Men, "A multi-period optimal power flow model including battery storage," 2013 IEEE *Power & Energy Soc. General Meeting*, pp.1-5, 2013.

[39] Y. Tao, Z. Xu, A. P. Meliopoulos and Z. Hu, "Optimal power flow with flexible loading," 2013 IEEE Power & Energy Society General Meeting, 2013, pp. 1-5, doi: 10.1109/PESMG.2013.6672370.

[40] Chen, T., Jin, Y., Lv, H.et al, "Applications of Lithium-Ion Batteries in Grid-Scale Energy Storage Systems". Trans. Tianjin Univ. 26,208-217, 2020.https://doi.org/10.1007/s12209-020-00236.
[41] Y. Wen, C. Guo, D. S. Kirschen, and S. Dong, "Enhanced security-constrained OPF with distributed battery energy storage," *IEEE Trans. on Power Sys.*, vol. 30, no. 1, pp. 98–108, Jan 2015.
[42] J. Cao, W. Du, and H. Wang, "An Improved Corrective Security -Constrained OPF With Distributed Energy Storage," *IEEE Trans. on Power Sys.*, vol. 31, no. 2, pp. 1537–1545, March 2016.
[43] Gill, S., Kockar, I., & Ault, G. W. "Dynamic Optimal Power Flow for Active Distribution Networks". IEEE Transactions on Power Systems, 2014, 29(1), 121–131. doi:10.1109/tpwrs.2013.2279263.
[44] M. I. Alizadeh, M. Usman and F. Capitanescu, "Toward Stochastic Multi-period AC Security Constrained Optimal Power Flow to Procure Flexibility for Managing Congestion and Voltages," 2021 International Conference on Smart Energy Systems and Technologies (SEST), 2021, pp. 1-6.
[45] T. Smed, G. Andersson, G. B. Sheble and L. L. Grigsby, "A new approach to AC/DC power flow," in IEEE Transactions on Power Systems, vol. 6, no. 3, pp.1238-1244, Aug. 1991.
[46] G. Durga Prasad, P. Seshagiri Rao,"A heuristic method for the real-time load flow solution of integrated multiterminal AC-DC power systems", Electric Power Systems Research, Volume 28, Issue 2, Pages 139-147, 1993.
[47] Wang XF, Fang WL, Du ZC. Modern power system analysis. Beijing: Science Press; 2003. p. 180–201.
[48] Jia Cao, Zheng Yan, Jianhua Li, Lu Cao, "Impact of HVDC line on the convergence property of AC/DC power flow calculation", International Journal of Electrical Power & Energy Systems, Volume 83, 2016, Pages 140-148, ISSN 0142-0615.
[49] Rabiee A, Soroudi A. Stochastic multiperiod OPF model of power systems with HVDC-connected intermittent wind power generation. IEEE Trans. Power Deliv, Feb. 2014; 29(1):336-44.
[50] A. Rabiee, A. Soroudi and A. Keane, "Information Gap Decision Theory Based OPF With HVDC Connected Wind Farms," in IEEE Trans. on Power Systems, vol. 30, no. 6, pp. 3396-3406, Nov. 2015.
[51] Huebner. N, Schween N, Suriyah. M, H. Vincent, L. Thomas, "Multi-area Coordination of Security-Constrained Dynamic Optimal Power Flow in AC-DC Grids with Energy Storage, Advances in Energy System Optimization, 27- 40, Springer International Publishing, 2020.
[52] Storn R., Price K., "Differential evolution – a simple and efficient heuristic for global optimization over continuous spaces', J Global Optim., 1997, 11, pp. 341– 359.
[53] A.A. Abou El Ela, M.A. Abido, S.R. Spea, Optimal power flow using differential evolution algorithm, Electric Power Systems Research, Volume 80, Issue 7,2010, Pages 878-885, ISSN 0378-7796.
[54] S. Das and P. N. Suganthan, "Differential Evolution: A Survey of the State-of-the-Art," in IEEE Transactions on Evolutionary Computation, vol. 15, no. 1, pp. 4-31, Feb. 2011.
[55] Cai Z, Gong W, Ling CX, Zhang H, "A clustering-based differential evolution for global optimization". Appl Soft Comput 11(1):1363–1379, 2011.
[56] Wang Y, Cai Z, Zhang Q, Enhancing the search ability of differential evolution through orthogonal crossover. Inf Sci 185(1):153-177, 2012.
[57] Yinzhi Zhou, Xinyu Li, Liang Gao, A differential evolution algorithm with intersect mutation operator, Applied Soft Computing, Volume 13, Issue 1, Pages 390-401, 2013, ISSN 1568-4946.
[58] Vaisakh, K., & Srinivas, L. R. Evolving ant direction differential evolution for OPF with non-smooth cost functions. Engineering Applications of Artificial Intelligence, 2011, 24(3), 426–436. doi: 10.1016/j.engappai.2010.10.019.
[59] Shouheng Tuo, Junying Zhang, Xiguo Yuan, Longquan Yong, "A new differential evolution algorithm for solving multimodal optimization problems with high dimensionality". Soft Comp. 22(13):4361-4388, 2018.
[60] Arsalan, Q." Expected Security Cost Optimal Power Flow Using Parallel and Distributed computation", Ph.D. dissertation, Oklahoma, USA, 2007.
[61] National Renewable Energy Laboratory (NREL). Available at www.nrel.gov.

Appendices

Operating Specifications of Controllable Appliances

Appliance	Average power consumption	Time interval
PHEVs	1.1 kW	9 hrs
Dish Washers	0.7 kW	3 hrs
Water heaters	5.5 kW	2 hrs
Kettles	2.0 kW	1 hr

Proposed MDE control parameters data

MDE control parameters data	
Dimension of problem (M)	9
Population size (N_{pop})	5
number of generations (τ_{max})	500
mutation factor (F_s)	0.5
CR_{max}	100/M
CR_{min}	30/M
LAR_{max}	0.99
LAR_{min}	0.1
AS_{max}	$(u^{max}-u^{min})/10$
AS_{mid}	$(u^{max}-u^{min})/(1E+4)$
AS_{min}	$(u^{max}-u^{min})/(1E+15)$